Immobilization of Molecularly Imprinted Polymer Nanoparticles onto Surfaces Using Different Strategies: Evaluating the Influence of the Functionalized Interface on the Performance of a Thermal Assay for the Detection of the Cardiac Biomarker Troponin I

Jake McClements,[1] Patrick Marcel Seumo Tchekwagep, [1] Ana Luiza Vilela Strapazon,[2] Francesco Canfarotta,[3] Alan Thomson, [3] Joanna Czulak, [1] Rhiannon E. Johnson, [3] Katarina Novakovic, [1] Patricia Losada-Pérez, [4] Azfar Zaman, [5] Ioakim Spyridopoulos, [5] Robert D. Crapnell[6]*, Craig E. Banks, [6] and Marloes Peeters[1]*

[1]School of Engineering, Newcastle University, Merz Court, Claremont Road, NE1 7RU Newcastle upon Tyne, U.K

[2]Faculdade de Ciências Farmacêuticas, Universidade de São Paulo, Av. Lineu Prestes, 580, São Paulo, São Paulo 05508-900, Brazil

[3]MIP Diagnostics Ltd, The Exchange Building, Colworth Park, Sharnbrook, MK44 1LQ Bedford, U.K

[4]Experimental Soft Matter and Thermal Physics (EST) Group, Department of Physics, Université Libre de Bruxelles, Boulevard du Triomphe CP223, 1050 Brussels, Belgium

[5]Department of Cardiology, Freeman Hospital and Newcastle University, Translational and Clinical Research Institute, NE7 7DN Newcastle upon Tyne, U.K.

[6]Faculty of Science and Engineering, Manchester Metropolitan University, John Dalton Building, Chester Street, M1 5GD Manchester, U.K.

Corresponding

Email: marloes.peeters@newcastle.ac.uk; r.crapnell@mmu.ac.uk

Abstract

We demonstrate that a novel functionalized interface, where molecularly imprinted polymer nanoparticles (nanoMIPs) are attached to screen-printed graphite electrodes (SPEs), can be utilized for the thermal detection of the cardiac biomarker troponin I (cTnI). The ultrasensitive detection of the unique protein cTnI can be utilized for the early diagnosis of myocardial infraction (i.e., heart attacks), resulting in considerably lower patient mortality and morbidity. Our developed platform presents an innovative route to develop accurate, low-cost, and disposable sensors for the diagnosis of cardiovascular diseases, specifically myocardial infraction. A reproducible and advantageous solid-phase approach was utilized to synthesize high-affinity nanoMIPs (average size = 71 nm) for cTnI, which served as synthetic receptors in a thermal sensing platform. To assess the performance and commercial potential of the sensor platform, various approaches were used to immobilize nanoMIPs onto thermocouples or SPEs: dip coating, drop casting, and a covalent approach relying on electrografting with an organic coupling reaction. Characterization of the nanoMIP-functionalized surfaces was performed with electrochemical impedance spectroscopy, atomic force microscopy, and scanning electron microscopy. Measurements from an in-house designed thermal setup revealed that covalent functionalization of nanoMIPs onto SPEs led to the most reproducible sensing capabilities. The proof of application was provided by measuring buffered solutions spiked with cTnI, which demonstrated that through monitoring changes in heat transfer at the solid–liquid interface, we can measure concentrations as low as 10 pg L^{-1}, resulting in the most sensitive test of this type. Furthermore, preliminary data are presented for a prototype platform, which can detect cTnI with shorter measurement times and smaller sample volumes. The excellent sensor performance, versatility of the nanoMIPs, and reproducible and low-cost nature of the SPEs demonstrate that this sensor platform technology has a clear commercial route with high potential to contribute to sustainable healthcare.

Introduction

Cardiovascular diseases (CVDs) accounted for 45% of all deaths in Europe in 2017, equating to 3.9 million fatalities, and 25% of all deaths in the USA, resulting in 655,000 fatalities. (1,2) They produce immense health and economic burdens and are estimated to cost the EU €210 billion a year, in addition to being responsible for the loss of more than 64 million disability-adjusted life years. (2) CVDs encompass a range of disorders that affect the heart, of which stroke and myocardial infarction (MI) have the highest patient mortality and morbidity. MI, also known as a heart attack, occurs when there is a decrease or stop in the flow of blood to a part of the heart, which leads to myocyte necrosis. (3,4) Damage to the heart muscle is determined through the measurement of cardiac troponins, protein biomarkers that are unique to the heart. (5) Cardiac troponins I and T (cTnI and cTnT, respectively) are encoded by different genes, which makes them immunologically distinct; however, both have been reported as specific and sensitive biomarkers for MI. Furthermore, they are superior to creatine kinase-MB and myoglobin as indicators for myocardial necrosis. (6,7) They provide important diagnostic and prognostic information and therefore form cornerstone markers for diagnosis of MI, alongside family history and electrocardiogram measurements.

The current "gold standard" diagnostic test for MI involves immunoassays, either focused on cTnI or cTnT, with a typical limit of detection (LoD) of around 1 ng L^{-1}. (5,8) However, the choice of analyte can lead to significantly different responses, and these assays do not contain identical reference materials or the same antibody composition. Furthermore, these assays are of high cost due to the need of a lab environment and the use of antibodies as recognition elements and can suffer from long measurement times (>30 min). (9) The latter is crucial since time until diagnosis is strongly linked to mortality; research has shown that if patients are treated within the "golden hour", damage to the heart muscles is reversible. (10) We will overcome the inherent drawbacks of immunoassays, including lack of standardized tests, by directly replacing antibodies with molecularly imprinted polymer nanoparticles (nanoMIPs), which are polymeric recognition elements, in diagnostic assays. (11,12) Consequently, the proposed technology has the potential to address many significant issues currently associated with the treatment and diagnosis of CVDs, resulting in reduced costs to healthcare systems and improved patient outcomes.

In our previous work, we developed high-affinity nanoMIPs for emerging cardiac biomarkers ST2 and heart fatty acid-binding protein (H-FABP) that had the benefits of low cost, scalability, robustness, and biocompatibility. (13) Some studies have previously prepared MIP-based sensors for the detection of cTnI; (14,15) however, using nanoMIPs to detect cTnI remains unexplored. Traditionally, MIPs are formed through the polymerization of monomers and cross-linker monomers, which self-assemble

based on the interaction of functional groups present on the target molecule. (16) After polymerization, the target molecule is removed from the polymer matrix, leaving the immobilized monomers in place and creating binding sites specific for the size, shape, and functionalities of the target. (17,18) As receptors, MIPs have experienced a rise in popularity due to their favorable affinity, ease of manufacturing, low cost, and high levels of adaptability. (19,20) Furthermore, MIP hybrids such as adapterMIPs can be utilized to further improve sensing capabilities. (21−23) These favorable properties have resulted in MIPs being utilized for numerous sensing applications such as detection of medical biomarkers, (24) antibiotics, (25) microorganisms, (26) toxins, (27) and viruses. (28) However, MIPs do present some significant drawbacks; primarily, their preparation method can lead to heterogeneous binding affinity sites, template leaching, and slow binding kinetics. Thus, to optimize sensing performance, we use a straightforward and highly advantageous solid-phase synthesis approach for manufacturing nanoMIPs for cTnI, which involves the polymerization of monomers and cross-linkers around a template molecule that is covalently attached to a solid support. (29) The removal of unreacted monomers and low-affinity polymers with an initial low-temperature elution step allows for the high-affinity nanoMIPs to be subsequently collected at higher temperatures (∼60 °C). This produces nanoparticles with homogeneous binding sites that can compete with (and sometimes surpass) antibodies in terms of affinity and selectivity. (30) These nanoMIPs can be used in conjunction with the heat-transfer method (HTM), a thermal detection technique, to provide a sensor platform that offers fast, low-cost detection and straightforward analysis. (13,31) This read-out strategy relies on monitoring the thermal resistance (Rth) at the solid–liquid interface and has previously been used for biomolecule detection, (32) monitoring bacteria growth, (33) and measuring protein levels. (13)

However, in previous research, nanoMIPs were dip-coated onto thermocouples, which is experimentally simple but has a number of disadvantages. For example, it is difficult to ensure homogeneity in the adsorbed material layer, and the nanoMIPs are only physisorbed to the surface, leading to poor reproducibility. (34) This method is also not suitable for medical diagnostics, as it is commonplace to use disposable electrodes to avoid contamination. Consequently, to achieve this with functionalized thermocouples, either a new thermocouple is required per measurement, which is too expensive, or regeneration of the nanoMIPs is required, which is complex. In this manuscript, we evaluate different strategies for functionalization of the interface, which are more suitable for commercial applications in terms of sensor performance, cost, and production methods. This includes direct dip coating of cTnI nanoMIPs to thermocouples to act as a control, drop casting onto screen-printed electrodes (SPEs), and covalent functionalization of the nanoMIPs onto SPEs using electrografting of diazonium salts. Importantly, SPEs are of extremely low cost, disposable, and highly

reproducible, which provides key advantages in regards to commercialization and standardization. Furthermore, despite their considerable commercial potential, nanoMIP-functionalized SPEs have not yet been utilized for the detection of biomarkers. (35) We demonstrate that it is possible to determine the cardiac biomarker cTnI not only at physiologically relevant levels but at concentrations as low as 10 pg L–1, resulting in the most sensitive test of this type. (5,36) Furthermore, we provide preliminary data relating to a new platform design, which can significantly reduce measurement times and sample volumes. The presented results also provide a set of controls to improve diagnostic reliability.

The simple covalent coupling procedure in combination with the low cost and reproducibility of the SPEs significantly enhances the commercial prospects of the platform. Due to the versatility of the nanoMIPs, there is also considerable potential for expansion to a multimarker format, which can find applications in many areas beyond diagnostics such as in food, water, and building industries, in addition to environmental monitoring.

Experimental Section

2.1. Equipment and Reagents

Bovine serum albumin (BSA), d-(+)-glucose, potassium chloride (KCl), ferrocyanide, ferricyanide, cTnI, and cTnT were purchased from Sigma (Gillingham, UK). Hydrochloric acid (HCl), 1-ethyl-3-(3-dimethylaminopropyl) carbodiimide (EDC), N-hydroxysuccinimide (NHS), 4-aminobenzoic acid (4-ABA), and sodium nitrite were purchased from Fisher Scientific (Loughborough, UK). The peptide sequence used as a template for the manufacture of anti-cTnI nanoMIPs was obtained from Ontores Biotechnologies (Shanghai, China). Phosphate-buffered saline (PBS) solutions were made using PBS tablets (Sigma) and deionized (DI) water (resistivity ≥ 18.2 MΩ cm).

To produce the screen-printed graphite macroelectrodes (3.1 mm diameter; SPEs), a carbon–graphite ink formulation (product code: C2000802P2; Gwent Electronic Materials Ltd., UK) was screen-printed onto a standard polyester substrate and cured at 60 °C for 30 min with a dielectric. (37) Chemicals and equipment for the synthesis and analysis of the nanoMIPs are presented in Canfarotta et al. (30)

2.2. Synthesis of cTnI NanoMIPs

The protocol was adapted from Canfarotta et al. (30) and was based on the epitope approach principle. Briefly, glass beads (diameter between 70 and 100 μm) were activated with 2 M sodium hydroxide and subsequently functionalized with an amino silane to obtain beads with free amine groups on the surface. In order to save on protein usage, the epitope approach was exploited; in particular, the molecule used as a template for imprinting is an epitope of cTnI, which was immobilized onto the amine-derivatized glass beads via succinimidyl iodoacetate coupling. Immobilization of the peptide was confirmed by monitoring color changes with a bicinchoninic acid assay. NanoMIPs were prepared according to a proprietary modified version of the protocol described in Canfarotta et al., (30) which involves radical polymerization of functional and cross-linker monomers at room temperature for 1 h. After polymerization, the solid support was used to isolate the high-affinity nanoMIPs from the remaining monomers, oligomers, and low-affinity polymers. This was achieved using first a low-temperature elution followed by an elevated-temperature elution (∼60 °C). (29)

2.3. Characterization of cTnI NanoMIPs

Size analysis was carried out using a NanoSight NS300 device (NanoSight Ltd., Malvern, UK) equipped with NanoSight NTA 3.4 software. Samples were first dialyzed using a SnakeSkin (Fisher Scientific, Loughborough, UK) dialysis membrane (molecular weight cut-off = 10 kDa) and diluted in DI water to a concentration of approximately 108 particles mL^{-1} prior to injection into the aforementioned device at room temperature (22.8 °C). Five independent analyses were performed, recording 60 s videos. The

nanoparticles were tracked using NTA software, which evaluates Brownian motion in solution. Brownian motion depends on the size of the particles, allowing the software to calculate the particle size.

2.4. Immobilization of NanoMIPs

We explored three different functionalization strategies (Scheme 1) to facilitate a comprehensive comparison of sensor performance and commercial potential. Although all three strategies are conventional, the dip coating method is not suitable for commercial applications due to the numerous aforementioned reasons. However, previous research has shown that this method exhibits favorable sensor performance with similar biomarkers, and therefore, it acted as a control. (13) In contrast, the SPEs prepared via drop casting and electrografting have significant potential for commercial use due to their low-cost and disposable nature. Therefore, it is important to compare their sensor performance to that of a previously established platform.

2.5. Dip Coating Thermocouples

Type K thermocouples (RS Components, Northamptonshire, UK) were exposed to solutions of nanoMIPs in water for 1 min with an insertion and withdrawing rate of 5.1 cm min–1. After drying under ambient conditions (2 h), the nanoMIP-functionalized thermocouples were inserted into 3D-printed flow cells, where the HTM measurement takes place.

2.6. NanoMIP-Functionalized SPE Preparation

SPEs were functionalized using two different methods. In the first one, 8 µL of the nanoMIP solution was directly drop-cast onto the SPE's working electrode. The SPEs were then left overnight (∼16 h) to allow the droplets to dry onto their surfaces. Following this, the SPEs were stored in PBS at 4 °C prior to use. The second method involved preparing a solution of 4-ABA (2 mM) and sodium nitrite (2 mM) in aqueous HCl (0.5 M) and gently mixing on an orbital shaker for 10 min. Following this, the SPEs were submerged into the solution, and cyclic voltammetry was performed (see the Supporting Information Figure S1 for the typical plot) from +0.2 V to −0.6 V at 100 mV s^{-1} using an Ag/AgCl reference electrode (Alvatek Ltd., Romsey, UK). The obtained electrode denoted as SPE/4-ABA was thoroughly rinsed with DI water to remove any unbound 4-ABA and dried with nitrogen. The carboxyl group was then activated through incubation with a solution of EDC (100 mM) and NHS (20 mM) in PBS buffer (pH = 5). Drop casting was utilized to deposit 8 µL of the EDC/NHS solution onto the working electrode of the SPEs. After 1 h, the electrodes were rinsed with DI water and dried to obtain the SPE/4-ABA/EDC + NHS electrodes. Following this, 8 µL of the nanoMIP solution was deposited onto the working

electrodes, following a gentle vortex. After 3 h, the nanoMIP solution was removed, and the electrode was dip-coated in 1% w/w BSA in PBS for 30 min to prevent non-specific binding to the surface. Finally, the SPE/4-ABA/EDC + NHS/nanoMIP electrodes were rinsed in DI water and dried with a gentle stream of nitrogen before being stored in PBS at 4 °C until use.

2.7. Characterization of NanoMIP-Functionalized SPEs

All electrochemical impedance spectroscopy (EIS) measurements were carried out using a PalmSens4 potentiostat (PalmSens, Houten, Netherlands) with a frequency range of 0.1 Hz–100 kHz. The experiments were performed in PBS with 1 mM ferricyanide, 1 mM ferrocyanide, and 0.1 M KCl.

Scanning electron microscopy (SEM) measurements were recorded on a Supra 40VP (Carl Zeiss Ltd., Cambridge, UK) with an average chamber and gun vacuum of 1.3×10^{-5} and 1×10^{-9} mbar, respectively. Samples were mounted onto aluminum SEM pin stubs (12 mm diameter, Agar Scientific, Essex, UK). To enhance contrast, a thin layer of Au/Pd (8 V, 30 s) was sputtered onto the electrodes using a SCP7640 coater (Polaron, Hertfordshire, UK).

Atomic force microscopy (AFM) measurements were performed on a JPK Nanowizard 4 BIO (Bruker, Nano GmbH, Berlin, Germany). Measurements were carried out in DI water to assess the nanoMIPs in their hydrated state. MLCT-E probes (Bruker, Santa Barbara, Ca, USA) were used with a quoted cantilever length of ∼0.55 µm, resonance frequency of ∼38 kHz, and spring constant of ∼ 0.1 N/m. All experiments were carried out at room temperature using the quantitative imaging mode.

2.8. Thermal Measurements of cTnI Using NanoMIP Sensor Platforms

Two separate 3D-printed flow cells were used within this work to facilitate measurements with both thermocouples and SPEs. The first flow cell, adapted from Crapnell et al., (13) enabled three thermocouples to be mounted in a single chamber, which allowed simultaneous measurements of multiple nanoMIP-functionalized thermocouples. This embedded a direct control into the system, in addition to allowing the selectivity of the platform to be assessed by comparing the response of cTnI nanoMIPs and H-FABP (another important cardiac biomarker) nanoMIPs to increasing concentrations of cTnI. In the second flow cell (Figures S2 and S3), one nanoMIP-functionalized electrode was mounted into the cell, and a thermocouple measured the temperature in the liquid (T2). For each measurement, a freshly prepared nanoMIP-functionalized electrode was used. The selectivity of these electrodes was examined by comparing the response of the nanoMIP designed for cTnI towards cTnT, which is similar in structure (Figures S4 and S5A). Additionally, the selectivity of the SPE prepared via electrografting was assessed further through exposure to both BSA and glucose (Figure S5).

The general protocol for the thermal measurements was very similar for both types of flow cells. The flow cells were connected to a heat-transfer device as described by van Grinsven et al. (38) The device was steered with LabView software that actively controls the temperature of the heat sink (copper block, T1), which was set to 37.00 ± 0.02 °C to mimic in vivo conditions. A proportional–integral–derivative (PID) controller attached to a power resistor (22 Ω) regulated the feedback on the signal. (39) The PID parameters were fixed for all experiments at optimized values of P = 1, I = 14, and D = 0.3.

In all measurements, the flow cells were filled with PBS and left for 45 min to ensure stabilization of the baseline temperature signal. Solutions (3 mL) of the target biomarker (cTnI 0–50 ng L–1) were prepared in PBS prior to experiments and stored at 4 °C until required. Each biomarker injection was performed at 250 µL min^{-1} for 12 min using an automated NE500 programmable syringe pump (ProSense, Oosterhout, the Netherlands) for the first-flow cell experiments and a LSP02-1B dual-channel syringe (Longer Precision Pump Co., Hebei, China) pump for the second-flow cell experiments. Following each sample addition, the system was allowed to stabilize for 30 min prior to the next injection. The Rth was determined throughout the experiments by dividing the temperature gradient (T1 – T2) over the power required to keep the heat sink at 37.00 °C. The Rth and standard deviation (SD) were calculated using the average of 600 data points from the baseline signal of each concentration and the initial PBS injection, respectively. These data were used to construct dose–response curves, from which the LoD was calculated using the three-sigma method in the linear range of the sensor. The error bars in the graphs relate to the SD values.

The cTnI concentration ranges were adjusted for each sensor platform to account for the different functionalization techniques. For example, the cTnI range was largest for the dip-coated thermocouples (0–50 ng L^{-1}) because they had greater surface areas compared to the SPEs and therefore more available binding sites, resulting in saturation occurring at higher concentrations. The cTnI ranges for the nanoMIP-functionalized SPEs prepared via drop casting and electrografting were 0–1 and 0–2 ng L^{-1}, respectively. These ranges are smaller than those of the thermocouples due to the lower surface area of the SPE's working electrodes. The cTnI range was smallest for the drop-cast SPEs, as the nanoMIPs were only physisorbed to the surface, which means that some nanoMIP desorption was likely, resulting in fewer binding sites at the electrode surface and thus saturation at lower concentrations. The starting concentrations for the SPEs were also lower compared to those of the thermocouples in order to further evaluate the specificity of the sensor platforms. Importantly, the response of each sensor type was measured at a cTnI concentration of 1 ng L^{-1}, which allowed for direct comparison of the sensor's performance at a fixed and physiologically relevant level.

Preliminary results were also obtained for a prototype 3D-printed manual addition cell, which is designed so that a syringe pump is not required to push liquid through the cell during the experiments. Instead, 100 µL of PBS/spiked PBS is simply added to and removed from a reservoir in the cell using a pipette. This method significantly reduces sample volumes (smaller by a factor of 30) and measurement times (faster by a factor of 3). The preliminary data were obtained using a nanoMIP-functionalized SPE prepared via electrografting and exposed to PBS containing cTnI (0–1 ng L^{-1}).

Results and Discussion

3.1. Production and Characterization of cTnI NanoMIPs

Following their production, nanoMIPs were subject to dialysis against DI water in order to remove any potential contaminants collected with the hot fraction. Afterward, the cTnI nanoMIPs were analyzed using NanoSight in DI water at room temperature (22.8 °C). As reported in Figure S6, the analysis revealed an average size of 71 nm (mode peak at 56 nm).

3.2. Characterization of NanoMIP-Functionalized SPEs

EIS was utilized to characterize SPEs at each stage of the covalent coupling process outlined in the Experimental Section (Figure 1).

A simple Randles equivalent circuit was used to fit the electrical parameters of the EIS results at each preparation step (Table S1). As illustrated in the inset of Figure 1B, the circuit includes the electrolyte resistance (Rs), double-layer capacitance (Cdl), Warburg impedance (W), and charge-transfer resistance (RCT). The Nyquist plots in Figure 1 clearly demonstrate that the RCT at the interface increases with each step of the coupling process. The bare SPE exhibits a small semicircle domain with an RCT of 6.7 kΩ. After the electrografting of 4-ABA, the RCT increases considerably to 10.2 kΩ due to the self-assembled layer of 4-ABA immobilized on the SPE. Following the activation of the carboxylic groups on the SPE, the RCT increases further to 12.6 kΩ. After the nanoMIPs were immobilized on the SPE, the RCT increases significantly to 16.8 kΩ. The reason for this trend is that all material deposited on to the SPE is essentially nonconductive, making electron transfer increasingly more difficult. Overall, the EIS results indicate that nanoMIPs were successfully immobilized on to the SPE using this preparation method.

3.3. SEM and AFM Characterization of NanoMIP-Functionalized SPEs

Imaging analysis corresponds with the EIS results and confirms that nanoMIPs were adsorbed to the SPE surfaces. SEM images (Figure 2) show that the SPE surfaces are relatively rough with a layer of binding agent (used for production) and some exposed graphite flakes. Due to the low-cost and disposable nature of SPEs, they cannot be produced with extremely flat surfaces, which makes imaging characterization more difficult. For example, as the binding agent is similar in size to the nanoMIPs, it is difficult to differentiate between the two materials. However, larger cTnI nanoMIPs are clearly visible in the SEM images for both functionalization strategies, and therefore, it can be assumed that smaller nanoMIPs are also adsorbed in larger numbers, thus corresponding to the size analysis and EIS results. Additional images of the functionalized and blank SPEs are presented in Figures S7 and S8 of the Supporting Information.

AFM was utilized to image the SPEs at smaller length scales in DI water (see Figure S9 for typical images). It was also generally difficult to differentiate between the nanoMIPs and binding agent on the surfaces from height images. However, by imaging areas of the SPEs with less binding agent, nanoMIPs were identified from stiffness images. Clear contrast was observed in the stiffness images, highlighting numerous particles on the surface. The images demonstrate that the particles had lower Young's modulus than the surrounding surface, which is expected for a nanoMIP, and their sizes ranged from 97 to 340 nm. Profile plots of the particles also revealed that their cross-sections fitted well to spherical caps, which is typical of an adsorbed nanoparticle (Figure S10). Consequently, these results confirm the presence of nanoMIPs at the surface. In regards to imaging characterization, the large surface roughness and binding agent present inherent drawbacks of SPEs as a material. However, ultra-flat surfaces are far more expensive to produce, which would significantly hinder the commercial prospects of the technology. Furthermore, the high surface roughness of the SPEs also presents an advantage through increased surface area, leading to more potential binding sites.

Through the combination of characterization techniques and HTM measurements, we can confirm the adsorption of nanoMIPs on the SPE surfaces via both drop casting and electrografting. Although beyond the scope of the current study, an interesting avenue for future research is AFM imaging the adsorbed nanoMIPs on an atomically flat surface in DI water. This would facilitate a novel and comprehensive characterization of the nanoMIPs in their hydrated state. (40,41)

3.4. Thermal Measurements of cTnI Using Different NanoMIP Sensor Platforms

To evaluate the specificity of the dip-coated thermocouple nanoMIP-based sensors, nanoMIPs for H-FABP (synthesis described by Crapnell et al. (13)) were functionalized onto another set of thermocouples. These thermocouples, in addition to blank thermocouples, were subsequently inserted into the 3D-printed flow cells and exposed to PBS solutions with increasing cTnI concentrations. The influence of the position of the functionalized thermocouples was determined in previous work; due to different positions in the liquid, the starting Rth value is different. (13) Consequently, the H-FABP nanoMIP, cTnI nanoMIP, and unfunctionalized thermocouples were placed in the front, middle, and back slots of the flow cell, respectively. Figure 3 presents typical data from the thermal measurements, demonstrating that the cTnI nanoMIP-functionalized thermocouples are able to detect this cardiac biomarker with high selectivity and specificity.

The cTnI nanoMIP-functionalized thermocouple stabilized in PBS at 3.09 °C W–1 with a SD of 0.95%. When cTnI was introduced at a concentration of 1 ng L^{-1}, a significant increase of 6.1% was observed

in the Rth. A linear increase occurs in the concentration range 0–10 ng L^{-1} with a maximum increase of 20.5% at a concentration of 50 ng L^{-1}. In contrast, the blank electrode does not show any response at this concentration, and the increase in the H-FABP nanoMIP-functionalized thermocouple is not significant. Hence, Figure 3 demonstrates that the observed change in Rth is due to the binding of cTnI to the cTnI nanoMIPs and therefore highlights the specificity and selectivity of the sensor platform. A LoD of 0.55 ± 0.14 ng L^{-1}1 was calculated, which is similar to that in our previous work on nanoMIP-functionalized thermocouples and classifies the sensor platform as an ultra-high sensitivity test. (5,13)

Although the thermocouple sensor platform exhibits favorable specificity and selectivity, it has a number of aforementioned disadvantages related to commercialization. Consequently, these results acted as a control, whereby the performance of the disposable SPE-based sensors could be compared against. SPEs, like thermocouples, exhibit a rough surface, which enables immobilization of the nanoMIPs between groves in the different graphite sheets by drop casting. While drop casting is traditionally used in combination with electrochemistry measurements, (42,43) the advantage of using thermal analysis is that it can monitor binding over the whole surface including the binder areas (a significant proportion of the electrode) which are not conductive.

Figure 4 presents the typical thermal response of the cTnI nanoMIP-functionalized SPEs prepared via drop casting upon addition of cTnI (5–1000 pg L^{-1}) in PBS. As stated within the Experimental Section, the starting concentration and concentration ranges were lower compared to those of the thermocouple-based sensor to further examine the platform specificity and make adjustments for the functionalization method, respectively.

Figure 4 demonstrates that the nanoMIP-functionalized SPE prepared via drop casting stabilized at an Rth value of 5.63 °C W^{-1} with a SD of 0.94%, which was similar to the measured noise on the thermocouple-based sensors. Furthermore, a comparable increase in Rth is observed across an equal cTnI concentration for both sensor types. For example, at 1 ng L^{-1}, the drop-cast SPE and dip-coated thermocouple experienced similar Rth increases of 4.9 and 6.1%, respectively. The smallest obtained LoD value was 10 pg L^{-1}, which is not only superior to that of the thermocouple-based sensor but makes the test the most sensitive one of its type. (36) Despite this favorable performance, triplicate measurements revealed that the sensor platform exhibited significant variation in its sensing capabilities. For example, the variation in the initial Rth value was large (range of 3.1 °C W^{-1}) and the LoD ranged from 10 to 30 pg L^{-1}. This variation is consistent with drop casting as the nanoMIPs are only physisorbed to the surface, which means that they are prone to desorption both before and during the experiments. This poor reproducibility would limit the sensor platform's commercial applications.

Thus, it is necessary to turn to covalent functionalization of the SPE surface. This was achieved by a simple procedure involving electrografting on the surface followed by EDC coupling of the nanoMIPs. Finally, BSA was added in order to prevent non-specific binding of cTnI to the surface. Figure 5 shows that there is a consistent linear change in the signal when the nanoMIP-functionalized SPE is exposed to increasing concentrations of cTnI (0.1–1.0 ng L^{-1}), after which saturation occurs due to growing occupation of the binding sites. Compared to the drop-cast SPEs, there is less variation between individually prepared electrodes, which is critical for commercial applications.

The nanoMIP-functionalized SPE prepared by electrografting stabilized at 2.49 °C W^{-1} with a SD of 0.99%. At a cTnI concentration of 1 ng L^{-1}, there is an Rth increase of 5.8%, which is very similar to that of the functionalized thermocouple (6.1%) and slightly greater than that of the drop-cast SPE (4.9%). A LoD of 0.46 ± 0.07 ng L^{-1} was achieved for the sensor, which is lower than that of the functionalized thermocouple but higher than that of the drop-cast SPE. However, despite this, the measured LoD places this sensor platform in the ultra-high sensitivity category and is superior to the vast majority of other cTnI tests. (5,36) The initial Rth values for the drop-cast and electrografted SPEs were 5.6 and 2.5 °C W–1, respectively. The reason for this difference is partly due to the difference in the amount of nanoMIPs on the SPE surface, in addition to a small change in the experimental setup where an additional support was needed to seal off the flow cell. Compared to the drop-cast SPEs, the SPEs prepared via electrografting produced more consistent results with lower variation in the initial Rth (range of 1.5 °C W^{-1}) and LoD (error of 15 vs 32%). This difference in consistency arises due to the different functionalization strategies. Through drop casting, the nanoMIPs are only physisorbed to the SPE surface, making desorption likely and therefore increasing variation in performance. In contrast, through electrografting, the nanoMIPs are covalently coupled to the SPE surface, which produces more consistent results. A highly reproducible sensor performance is crucial for commercial applications, and therefore, the electrografted SPE platform possesses the greatest commercial potential.

The selectivity of both SPE-based sensors was examined by repeating the HTM experiments using cTnT (Figures S4 and S5A). The results demonstrated that both SPE sensors exhibited good selectivity, as only a very limited increase in Rth occurred when cTnT replaced cTnI. Additionally, in order to further assess the selectivity of the optimal sensor platform (SPE prepared via electrografting), experiments were performed using BSA and glucose at physiologically relevant concentrations (Figure S5). The results showed that the Rth only experienced a very small increase upon exposure to BSA and a marginal increase upon exposure to glucose despite its concentration being a factor of 109 larger than that of cTnI in order to mimic levels within the blood. These results further demonstrate the favorable

selectivity of the SPE sensor prepared via electrografting, which presents a promising outlook for commercialization.

Table 1 presents an overview of the key performance parameters of each sensor type. The results demonstrate that all three functionalization methods led to sensors with high specificity and selectivity. Clinically relevant assays should be able to measure variations of 1 ng L^{-1} cTnI (with a baseline of 1 ng L^{-1}) with a maximum SD of 5%. (8) Consequently, all three developed sensors significantly exceed these clinical standards. However, the SPE prepared via electrografting showed the most promising results. The platform had similar sensing capabilities to the thermocouple-based sensor but was far more commercially viable due to its low cost and disposability. Furthermore, the sensor platform produced more consistent results than the drop-cast SPE, which is directly related to the functionalization method. The LoD of the electrografted nanoMIP-based sensor was superior to that in many other recently developed tests for cTnI (see Table S2 for full comparison). (14,36,44,45) Crucially, it also uses components which are significantly lower in cost. For example, many cTnI tests utilize gold electrodes, graphite quantum dots, glassy carbon electrodes, and carbon nanotubes within their platforms. (14,44,45) These components are orders of magnitude more costly compared to carbon SPEs. This highlights the significant commercial promise of the developed sensor platform for diagnosis of MI, in addition to many other areas beyond diagnostics.

Finally, preliminary experiments were performed using a 3D-printed manual addition cell, in which a smaller volume of liquid was injected into and removed from the cell by the user. This led to a reduction in sample volume from 3 mL to 100 µL, in addition to measurement times decreasing by a factor of 3 with potential for further improvements. These two factors are extremely important in relation to the commercial applications of the sensor platform, and thus, any improvements are significant. The HTM data for the prototype manual addition cell using a nanoMIP-functionalized SPE prepared via electrografting are presented within the Supporting Information (Figure S11). The results demonstrate that upon exposure to a cTnI concentration of 1 ng L^{-1}, the Rth increased by 5.3%, which is similar to that in the other platforms. However, the measured SD of the baseline and LoD were 1.33% and 0.76 ± 0.11 ng L^{-1}, respectively. Therefore, despite meeting clinical standards, (8) the sensor performance is inferior to that of the flow cell SPE-based platforms. These initial results provide an interesting avenue for future work in order to optimize the sensor performance of the prototype platform and therefore further increase the commercial viability of the technology.

Conclusions

High-affinity cTnI nanoMIPs were manufactured according to a solid-phase approach. The nanoMIPs were immobilized onto thermocouples via dip coating and SPEs via drop casting or electrografting. NanoMIP-functionalized thermocouples have previously been developed for similar cardiac biomarkers and exhibited favorable performance but poor commercial viability. In contrast, SPEs are highly reproducible, of low cost, and disposable, which has significant benefits for medical diagnostics by avoiding cross-contamination and allowing for simple commercialization. Furthermore, this manuscript is the first report on combining nanoMIPs with SPEs as an electrode material to detect a biomarker. The sensing capabilities of the developed SPE sensors were evaluated and compared to those of the thermocouple-based sensor.

Before the HTM experiments, the SPEs were characterized using a combination of EIS, SEM, and AFM, which confirmed the presence of adsorbed nanoMIPs at their surfaces. However, the nanoMIPs were difficult to identify due to the binding agent also present on the SPE surfaces. Following characterization, the SPEs and thermocouples were inserted into tailored 3D-printed flow cells and exposed to buffered solutions spiked with increasing amounts of cTnI. The starting cTnI concentration and concentration ranges were adjusted to account for the different functionalization strategies of each sensor platform. A home-made thermal measurement device was coupled to the flow cells and utilized to measure the change in Rth at the solid–liquid interface for increasing concentrations of cTnI.

The flow cell used for the thermocouples was a multimarker platform, which enabled the simultaneous measurements of cTnI nanoMIP-functionalized and H-FABP (a similar cardiac biomarker) nanoMIP-functionalized thermocouples, in addition to an unfunctionalized thermocouple, which acted as a control. A significant increase in Rth upon exposure to cTnI was achieved for the cTnI nanoMIP thermocouple, while the response for the H-FABP nanoMIP thermocouple was not significant. This demonstrated that the platform was able to measure cTnI with high specificity (LoD = 0.55 ± 0.14 ng L^{-1}) and selectivity. While this is within the physiologically relevant range and classed as an ultra-high sensitivity test, the method neither allows for controlled deposition of the nanoMIPs on the surface nor is it compatible with mass production.

We demonstrated that the functionalization procedure is crucial when preparing SPEs in order to achieve high specificity and reproducibility. Drop casting nanoMIPs onto SPEs led to the lowest LoD values (<30 pg L^{-1}) but high variation (Rth range of 3.1 °C W^{-1}) between individual electrodes. A novel, yet simple strategy based on electrografting of diazonium salts combined with standard EDC coupling produced a more consistent sensor performance. The sensor platform was able to determine

medically relevant levels of cTnI and variations therein. Furthermore, it had a superior LoD to that in the dip coating approach, in addition to many other recently developed high-cost tests for cTnI. The selectivity of this method was confirmed by evaluating the thermal response to cTnT. In the future, these results will be benchmarked by measuring (frozen) serum samples, of which the concentration has previously been determined by immunoassays. The sensing capabilities of a prototype manual addition cell using a nanoMIP-functionalized SPE prepared via electrografting were also examined. Although sensor performance was inferior, the platform demonstrated key advantages in terms of measurement times and sample volumes. Therefore, this presents an interesting avenue for future research in order to further increase the commercial viability of the platform.

The use of nanoMIP-functionalized SPEs combined with thermal read-out has a clear route to commercialization. It has considerable potential for sustainable healthcare given that the approach is accurate, of low cost, scalable, and simple to operate, and nanoMIPs can be tailored toward virtually any target of interest.

Acknowledgments

P.M.S.T. and M.P. thank the Royal Society of Chemistry for the Researcher Mobility Grant (M19-7489). J.M. would like to acknowledge the Engineering and Physical Sciences Research Council (EPSRC) Impact Accelerator Account from Newcastle University for his salary. J.M.C., K.N., I.S., A.Z., and M.P. would also like to thank the Rosetrees Trust (Seedcorn2020\100303) for contribution toward consumables. We would like to thank Prof. Jonas Gruber (Universidade de São Paulo), supervisor of A.L.V.S., and Dr. Francesco Mecozzi (Manchester Metropolitan University) for insightful discussions regarding cardiac biomarker sensing.Scheme 1. Illustration of the Three Functionalization Strategies Used to Immobilize NanoMIPs onto Surfaces; (A) NanoMIPs are Physisorbed to a Thermocouple through Dip Coating; (B) NanoMIPs are Physisorbed to the Working Electrode of a SPE through Drop Casting; and (C) 4-ABA is Electrografted to the Working Electrode of a SPE and an EDC/NHS Coupling Reaction is then Utilized to Covalently Couple the nanoMIPs to the SPE Surface

References

1. Wilkins, E.; Wilson, L.; Wickramasinghe, K.; Bhatnagar, P.; Leal, J.; Luengo-Fernandez, R.; Burns, R.; Rayner, M.; Townsend, N. European Cardiovascular Disease Statistics; European Heart Network: Brussels, Belgium, 2017; Vol. 34.
2. Benjamin, E. J.; Blaha, M. J.; Chiuve, S. E.; Cushman, M.; Das, S. R.; Deo, R.; de Ferranti, S. D.; Floyd, J.; Fornage, M.; Gillespie, C.; Isasi, C. R.; Jiménez, M. C.; Jordan, L. C.; Judd, S. E.; Lackland, D.; Lichtman, J. H.; Lisabeth, L.; Liu, S.; Longnecker, C. T.; Mackey, R. H.; Matsushita, K.; Mozaffarian, D.; Mussolino, M. E.; Nasir, K.; Neumar, R. W.; Palaniappan, L.; Pandey, D. K.; Thiagarajan, R. R.; Reeves, M. J.; Ritchey, M.; Rodriguez, C. J.; Roth, G. A.; Rosamond, W. D.; Sasson, C.; Towfighi, A.; Tsao, C. W.; Turner, M. B.; Virani, S. S.; Voeks, J. H.; Willey, J. Z.; Wilkins, J. T.; Wu, J. H.; Alger, H. M.; Wong, S. S.; Muntner, P. Heart Disease and Stroke Statistics–2017 Update: A Report From the American Heart Association. Circulation 2017, 135, e146– e603,
3. Body, R.; Carlton, E. Understanding Cardiac Troponin Part 1: Avoiding Troponinitis. Emerg. Med. J. 2018, 35, 120– 125, DOI: 10.1136/emermed-2017-206812
4. Thygesen, K.; Alpert, J. S.; White, H. D. Universal Definition of Myocardial Infarction. J. Am. Coll. Cardiol. 2007, 50, 2173– 2195, DOI: 10.1016/j.jacc.2007.09.011
5. Galli, C.; Lippi, G. High-Sensitivity Cardiac Troponin Testing in Routine Practice: Economic and Organizational Advantages. Ann. Transl. Med. 2016, 4, 257, DOI: 10.21037/atm.2016.07.04
6. Archan, S.; Fleisher, L. A. From Creatine Kinase-MB to Troponin: The Adoption of a New Standard. Anesthesiology 2010, 112, 1005– 1012, DOI: 10.1097/aln.0b013e3181d31fa8
7. White, H. D.; Chew, D. P. Acute Myocardial Infarction. Lancet 2008, 372, 570– 584, DOI: 10.1016/s0140-6736(08)61237-4
8. National Institute for Health and Care Excellence. High-Sensitivity Troponin Tests for the Early Rule Out of NSTEMI , 2020.
9. Lippi, G.; Cervellin, G. Choosing Troponin Immunoassays in a World of Limited Resources. J. Am. Coll. Cardiol. 2013, 62, 647– 648,
10. Boersma, E.; Maas, A. C.; Deckers, J. W.; Simoons, M. L. Early Thrombolytic Treatment in Acute Myocardial Infarction: Reappraisal of the Golden Hour. Lancet 1996, 348, 771– 775,
11. Sharma, S.; Jackson, P. G.; Makan, J. Cardiac Troponins. J. Clin. Pathol. 2004, 57, 1025– 1026,
12. Ammann, P.; Pfisterer, M.; Fehr, T.; Rickli, H. Raised Cardiac Troponins. Br. Med. J. 2004, 328, 1028– 1029,
13. Crapnell, R. D.; Canfarotta, F.; Czulak, J.; Johnson, R.; Betlem, K.; Mecozzi, F.; Down, M. P.; Eersels, K.; Van Grinsven, B.; Cleij, T. J.; Law, R.; Banks, C. E.; Peeters, M. Thermal Detection of Cardiac Biomarkers Heart-Fatty Acid Binding Protein and ST2 Using a Molecularly Imprinted Nanoparticle-Based Multiplex Sensor Platform. ACS Sens. 2019, 4, 2838– 2845,
14. Yola, M. L.; Atar, N. Development of Cardiac Troponin-I Biosensor Based on Boron Nitride Quantum Dots Including Molecularly Imprinted Polymer. Biosens. Bioelectron. 2019, 126, 418– 424,
15. Zuo, J.; Zhao, X.; Ju, X.; Qiu, S.; Hu, W.; Fan, T.; Zhang, J. A New Molecularly Imprinted Polymer (MIP)-Based Electrochemical Sensor for Monitoring Cardiac Troponin I (CTnI) in the Serum. Electroanalysis 2016, 28, 2044– 2049,
16. Vasapollo, G.; Sole, R. D.; Mergola, L.; Lazzoi, M. R.; Scardino, A.; Scorrano, S.; Mele, G. Molecularly Imprinted Polymers: Present and Future Prospective. Int. J. Mol. Sci. 2011, 12, 5908– 5945,
17. Haupt, K.; Mosbach, K. Molecularly Imprinted Polymers and Their Use in Biomimetic Sensors. Chem. Rev. 2000, 100, 2495– 2504,

18. Sellergren, B.; Hall, A. J. Molecularly Imprinted Polymers Supramolecular Chemistry: From Molecules to Nanomaterials; Steed, J. W., Gale, P. A., Eds.; Wiley and Sons, Ltd: Chichester, 2012, pp 3255– 3282
19. Crapnell, R. D.; Dempsey-Hibbert, N. C.; Peeters, M.; Tridente, A.; Banks, C. E. Molecularly Imprinted Polymer Based Electrochemical Biosensors: Overcoming the Challenges of Detecting Vital Biomarkers and Speeding up Diagnosis. Talanta Open 2020, 2, 100018,
20. Uzun, L.; Turner, A. P. F. Molecularly-Imprinted Polymer Sensors: Realising Their Potential. Biosens. Bioelectron. 2016, 76, 131– 144,
21. Tang, W.; Li, G.; Row, K. H.; Zhu, T. Preparation of Hybrid Molecularly Imprinted Polymer with Double-Templates for Rapid Simultaneous Purification of Theophylline and Chlorogenic Acid in Green Tea. Talanta 2016, 152, 1– 8,
22. Sullivan, M. V.; Clay, O.; Moazami, M. P.; Watts, J. K.; Turner, N. W. Hybrid Aptamer-Molecularly Imprinted Polymer (AptaMIP) Nanoparticles from Protein Recognition—A Trypsin Model. Macromol. Biosci. 2021, 21, e2100002
23. Ayankojo, A. G.; Reut, J.; Öpik, A.; Furchner, A.; Syritski, V. Hybrid Molecularly Imprinted Polymer for Amoxicillin Detection. Biosens. Bioelectron. 2018, 118, 102– 107,
24. Özcan, N.; Karaman, C.; Atar, N.; Karaman, O.; Yola, M. L. A Novel Molecularly Imprinting Biosensor Including Graphene Quantum Dots/Multi-Walled Carbon Nanotubes Composite for Interleukin-6 Detection and Electrochemical Biosensor Validation. ECS J. Solid State Sci. Technol. 2020, 9, 121010,
25. Jamieson, O.; Soares, T. C. C.; de Faria, B. A.; Hudson, A.; Mecozzi, F.; Rowley-Neale, S. J.; Banks, C. E.; Gruber, J.; Novakovic, K.; Peeters, M.; Crapnell, R. D. Screen Printed Electrode Based Detection Systems for the Antibiotic Amoxicillin in Aqueous Samples Utilising Molecularly Imprinted Polymers as Synthetic Receptors. Chemosensors 2020, 8, 5,
26. Dar, K. K.; Shao, S.; Tan, T.; Lv, Y. Molecularly Imprinted Polymers for the Selective Recognition of Microorganisms. Biotechnol. Adv. 2020, 45, 107640,
27. Sergeyeva, T.; Yarynka, D.; Piletska, E.; Linnik, R.; Zaporozhets, O.; Brovko, O.; Piletsky, S.; El'skaya, A. Development of a Smartphone-Based Biomimetic Sensor for Aflatoxin B1 Detection Using Molecularly Imprinted Polymer Membranes. Talanta 2019, 201, 204– 210,
28. Bolisay, L. D.; Culver, J. N.; Kofinas, P. Molecularly Imprinted Polymers for Tobacco Mosaic Virus Recognition. Biomaterials 2006, 27, 4165– 4168,
29. Poma, A.; Guerreiro, A.; Whitcombe, M. J.; Piletska, E. V.; Turner, A. P. F.; Piletsky, S. A. Solid-Phase Synthesis of Molecularly Imprinted Polymer Nanoparticles with a Reusable Template-Plastic Antibodies. Adv. Funct. Mater. 2013, 23, 2821– 2827,
30. Canfarotta, F.; Poma, A.; Guerreiro, A.; Piletsky, S. Solid-Phase Synthesis of Molecularly Imprinted Nanoparticles. Nat. Protoc. 2016, 11, 443– 455,
31. Canfarotta, F.; Czulak, J.; Betlem, K.; Sachdeva, A.; Eersels, K.; van Grinsven, B.; Cleij, T. J.; Peeters, M. A Novel Thermal Detection Method Based on Molecularly Imprinted Nanoparticles as Recognition Elements. Nanoscale 2018, 10, 2081– 2089,
32. Betlem, K.; Mahmood, I.; Seixas, R. D.; Sadiki, I.; Raimbault, R. L. D.; Foster, C. W.; Crapnell, R. D.; Tedesco, S.; Banks, C. E.; Gruber, J.; Peeters, M. Evaluating the Temperature Dependence of Heat-Transfer Based Detection: A Case Study with Caffeine and Molecularly Imprinted Polymers as Synthetic Receptors. Chem. Eng. J. 2019, 359, 505– 517,
33. Betlem, K.; Kaur, A.; Hudson, A. D.; Crapnell, R. D.; Hurst, G.; Singla, P.; Zubko, M.; Tedesco, S.; Banks, C. E.; Whitehead, K.; Peeters, M. Heat-Transfer Method: A Thermal Analysis Technique for the Real-Time Monitoring of Staphylococcus Aureus Growth in Buffered Solutions and Digestate Samples. ACS Appl. Bio Mater. 2019, 2, 3790– 3798,

34. Brinker, C. J. Dip Coating. Chemical Solution Deposition of Functional Oxide Thin Films; Schneller, T. W., Kosec, M. R., Eds.; Springer: Vienna, 2013, pp 233– 261
35. Alanazi, K.; Garcia Cruz, A.; Di Masi, S.; Voorhaar, A.; Ahmad, O. S.; Cowen, T.; Piletska, E.; Langford, N.; Coats, T. J.; Sims, M. R.; Piletsky, S. A. Disposable Paracetamol Sensor Based on Electroactive Molecularly Imprinted Polymer Nanoparticles for Plasma Monitoring. Sens. Actuators, B 2021, 329, 129128,
36. Regan, B.; Boyle, F.; O'Kennedy, R.; Collins, D. Evaluation of Molecularly Imprinted Polymers for Point-of-Care Testing for Cardiovascular Disease. Sensors 2019, 19, 3485,
37. Galdino, F. E.; Foster, C. W.; Bonacin, J. A.; Banks, C. E. Exploring the Electrical Wiring of Screen-Printed Configurations Utilised in Electroanalysis. Anal. Methods 2015, 7, 1208– 1214,
38. van Grinsven, B.; Eersels, K.; Peeters, M.; Losada-Pérez, P.; Vandenryt, T.; Cleij, T. J.; Wagner, P. The Heat-Transfer Method: A Versatile Low-Cost, Label-Free, Fast, and User-Friendly Readout Platform for Biosensor Applications. ACS Appl. Mater. Interfaces 2014, 6, 13309– 13318,
39. Geerets, B.; Peeters, M.; van Grinsven, B.; Bers, K.; de Ceuninck, W.; Wagner, P. Optimizing the Thermal Read-out Technique for MIP-Based Biomimetic Sensors: Towards Nanomolar Detection Limits. Sensors 2013, 13, 9148– 9159,
40. McClements, J.; Zhang, M.; Radacsi, N.; Koutsos, V. Measuring the Interactions between Carbon Black Nanoparticles and Latex Thin Films in Aqueous Media Using AFM Force Spectroscopy. Colloids Surf., A 2020, 603, 124920,
41. McClements, J.; Buffone, C.; Shaver, M. P.; Sefiane, K.; Koutsos, V. Poly(Styrene-Co-Butadiene) Random Copolymer Thin Films and Nanostrucutres on a Mica Surface: Morphology and Contact Angles of Nanodroplets. Soft Matter 2017, 13, 6152– 6166,
42. Gui, R.; Guo, H.; Jin, H. Preparation and Applications of Electrochemical Chemosensors Based on Carbon-Nanomaterial-Modified Molecularly Imprinted Polymers. Nanoscale Adv. 2019, 1, 3325– 3363,
43. Garcia Cruz, A.; Haq, I.; Cowen, T.; Di Masi, S.; Trivedi, S.; Alanazi, K.; Piletska, E.; Mujahid, A.; Piletsky, S. A. Design and Fabrication of a Smart Sensor Using in Silico Epitope Mapping and Electro-Responsive Imprinted Polymer Nanoparticles for Determination of Insulin Levels in Human Plasma. Biosens. Bioelectron. 2020, 169, 112536,
44. Sharma, A.; Han, C.-H.; Jang, J. Rapid Electrical Immunoassay of the Cardiac Biomarker Troponin I through Dielectrophoretic Concentration Using Imbedded Electrodes. Biosens. Bioelectron. 2016, 82, 78– 84,
45. Dhawan, S.; Sadanandan, S.; Haridas, V.; Voelcker, N. H.; Prieto-Simón, B. Novel Peptidylated Surfaces for Interference-Free Electrochemical Detection of Cardiac Troponin I. Biosens. Bioelectron. 2018, 99, 486– 492,

Figure 1. (A) Nyquist plot for the EIS measurements of the bare SPE (black squares), 4-ABA electrografted on the SPE (red circles), activation of carboxylic groups (green triangles), and covalent coupling of nanoMIPs (blue inverted triangles). (B) Corresponding plot where modeling was performed with a Randles equivalent electrochemical circuit (see the inset), where the lines indicate the relevant fit data. Measurements were performed in PBS with 1 mM ferricyanide, 1 mM ferrocyanide, and 0.1 M KCl.

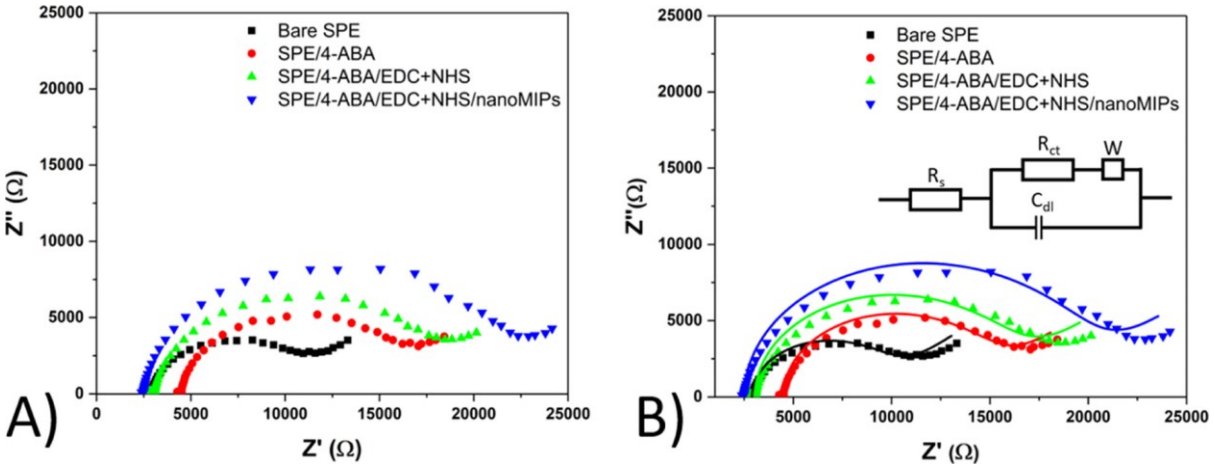

Figure 2. (A) SEM images of cTnI nanoMIP-functionalized SPEs prepared via (A) drop casting and (B) electrografting.

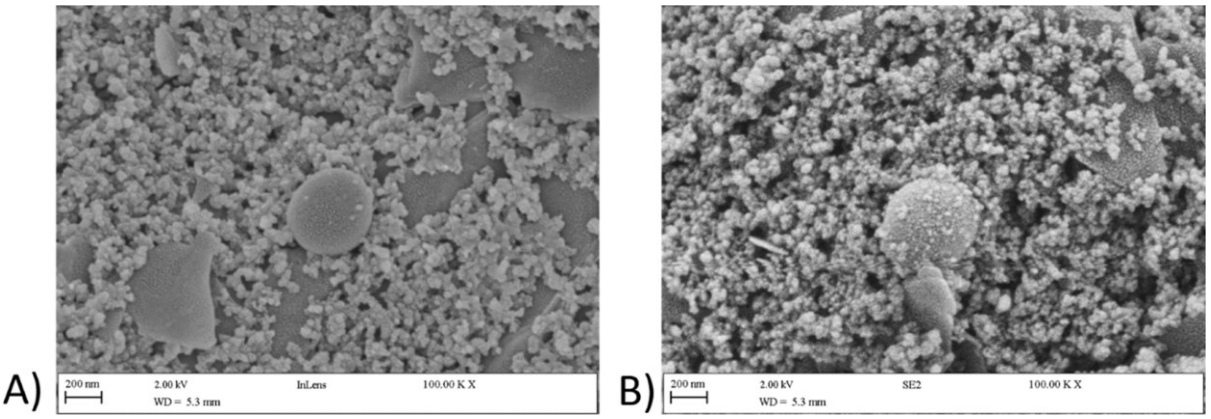

Figure 3. (A) Typical raw HTM data plot obtained (Rth vs time) for the addition of cTnI (1–50 ng L^{-1}) in PBS to cTnI nanoMIP-functionalized (red), H-FABP nanoMIP-functionalized (blue), and unfunctionalized thermocouples (black). (B) Corresponding scatter plot showing the change in Rth for the addition of cTnI in PBS to cTnI nanoMIP-functionalized (circles), H-FABP nanoMIP-functionalized (squares), and unfunctionalized thermocouples (triangles). (C) Corresponding dose–response plot for the cTnI nanoMIP-functionalized thermocouple with an allometric fit where the slope (a) = 6.14 ± 0.71 and allometric coefficient (b) = 0.31 ± 0.04.

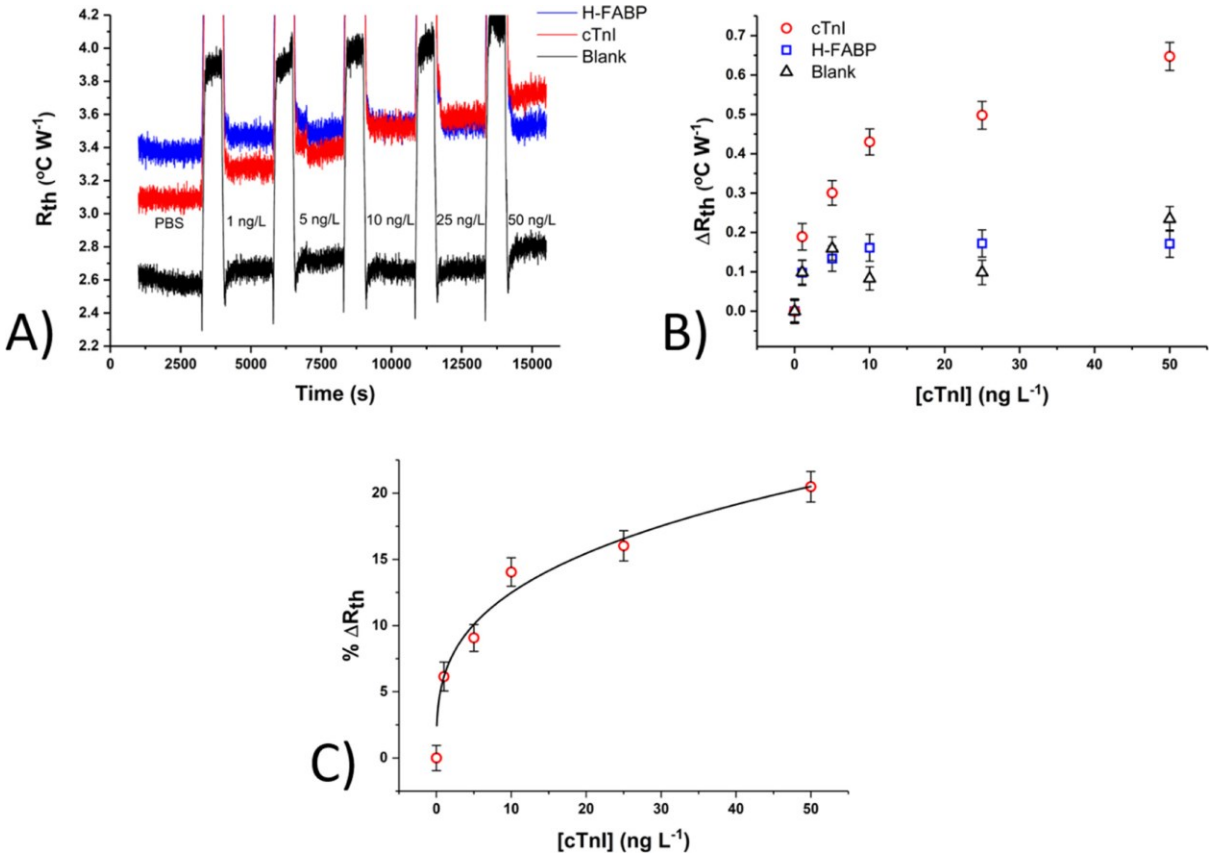

Figure 4. (A) Typical raw and smoothed HTM data (Rth vs time) for the nanoMIP-functionalized SPE prepared via drop casting upon exposure to PBS containing 5–1000 pg L^{-1} cTnI. The smoothed data were obtained using a 50-point percentile filter. (B) Corresponding scatter plot showing the change in Rth for the addition of cTnI in PBS. (C) Corresponding dose–response plot with an allometric fit where a = 1.82 ± 0.37 and b = 0.15 ± 0.04.

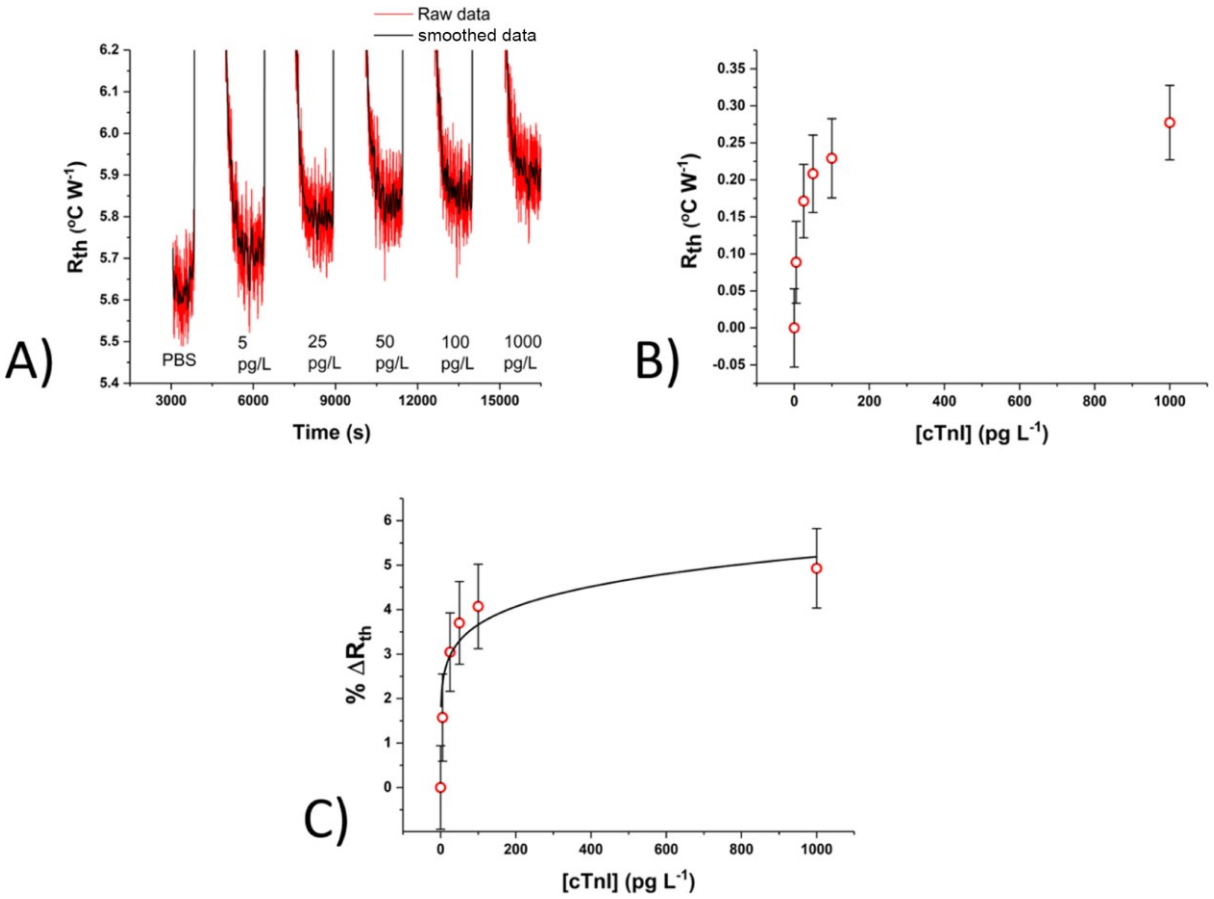

Figure 5. (A) Typical raw and smoothed HTM data (Rth vs time) for the nanoMIP-functionalized SPE prepared via electrografting upon exposure to PBS containing 0.1–2 ng L^{-1} cTnI. The smoothed data were obtained using a 50-point percentile filter. (B) Corresponding scatter plot showing the change in Rth for the addition of cTnI in PBS. (C) Corresponding dose–response plot with an allometric fit where a = 5.91 ± 0.06 and b = 0.61 ± 0.01.

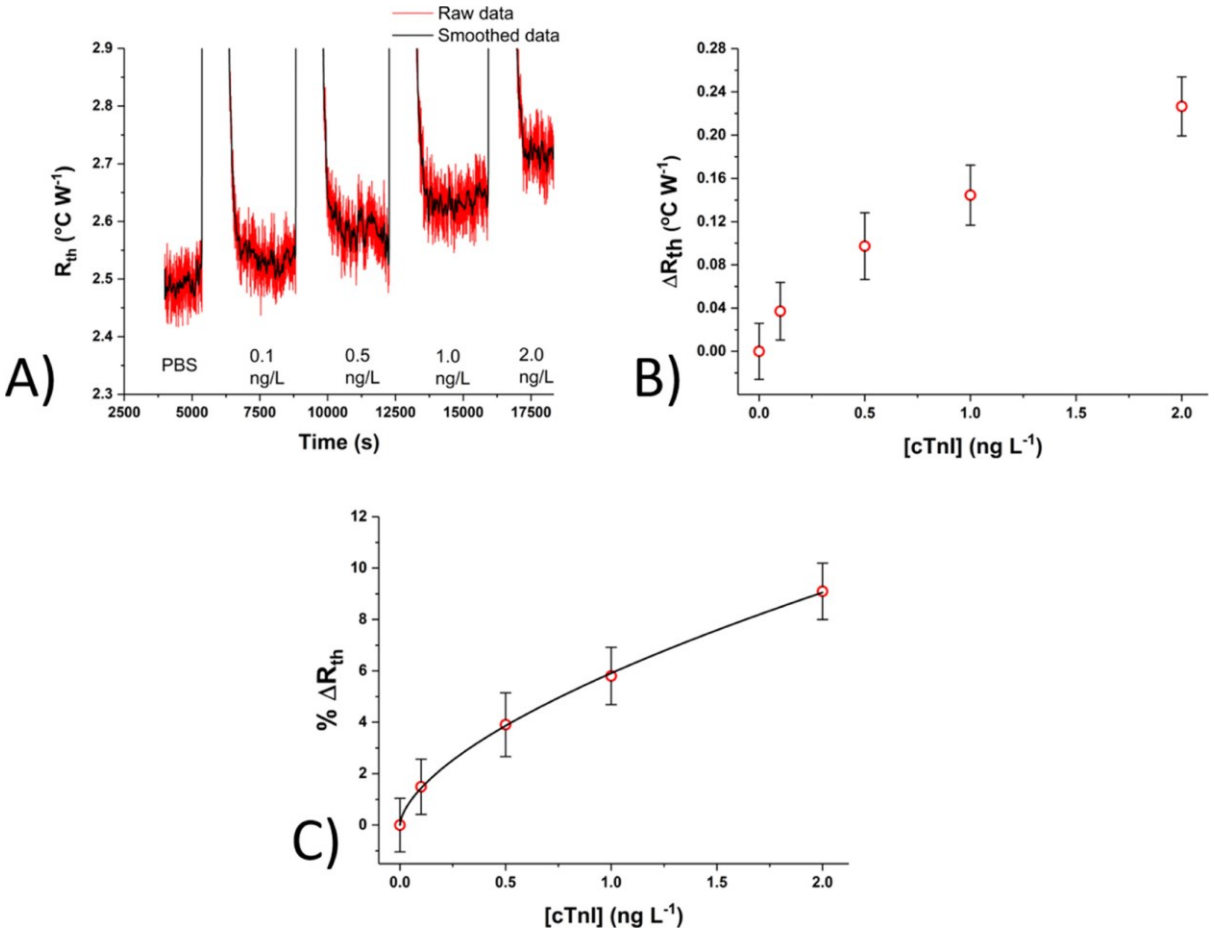

Table 1. Preparation Method and Performance Parameters of Each Sensor Type

sensor type	preparation method	SD (%)	ΔR_{th} at 1 ng L^{-1} (%)	maximum LoD (ng L^{-1}) (%)	range in starting R_{th} (°C W^{-1})
thermocouple	dip coating	0.95	6.1	0.55 ± 26	0.5
SPE	drop casting	0.94	4.9	0.03 ± 32	3.1
SPE	Covalent Coupling	0.99	5.8	0.46 ± 15	1.5